nature neuroscience

Serum response factor controls neuronal circuit assembly in the hippocampus

Bernd Knöll[1], Oliver Kretz[2], Christine Fiedler[1], Siegfried Alberti[1], Günther Schütz[3], Michael Frotscher[2] & Alfred Nordheim[1]

Higher organisms rely on multiple modes of memory storage using the hippocampal network, which is built by precisely orchestrated mechanisms of axonal outgrowth, guidance and synaptic targeting. We demonstrate essential roles of the transcription factor serum response factor (SRF), a sensor of cytoskeletal actin dynamics, in all these processes. Conditional deletion of the mouse *Srf* gene reduced neurite outgrowth and abolished mossy fiber segregation, resulting in ectopic fiber growth inside the pyramidal layer. SRF-deficient mossy fibers aberrantly targeted CA3 somata for synapse formation. Axon guidance assays showed that SRF was a key mediator of ephrin-A and semaphorin guidance cues; in SRF-deficient neurons, these resulted in the formation of F-actin–microtubule rings rather than complete growth cone collapse. Dominant-negative variants of the SRF cofactor megakaryocytic acute leukemia (MAL) severely impeded neurite outgrowth and guidance. These data highlight essential links between SRF-mediated transcription and axon guidance and circuit formation in the hippocampus.

Wiring the brain into functional circuits requires distinct neuronal outgrowth and pathfinding processes. To integrate and respond to guidance signals, navigating growth cones require highly dynamic cytoskeletal structures. The trisynaptic circuit of the hippocampal projection is well suited for studying neurite outgrowth and axon guidance. Mossy fiber axons—involved in nonassociative learning protocols[1] and in epileptic seizures[2]—emanate from dentate gyrus (DG) granule cells and bifurcate by a (thus far) unknown mechanism into supra- and infrapyramidal branches[3]. After bifurcation, these axons navigate in a precise manner on either side of the stratum pyramidale formed by CA3 pyramidal neurons until they synapse onto the apical dendrites of these neurons.

We analyzed the function of SRF, a MADS-box transcription factor, in neurite outgrowth, axon guidance and synaptic targeting. SRF mediates the rapid induction of immediate-early genes (IEGs) such as *Fos* and *Egr1* (ref. 4), cooperating with cofactors such as Ets-type or myocardin proteins (such as megakaryocytic acute leukemia, MAL), to regulate target gene expression[5–7].

Deleting SRF in mouse embryonic stem (ES) cells and in *Drosophila melanogaster* affects cell adhesion, spreading and migration[8,9]. SRF activity is intimately linked to cytoskeletal dynamics, in particular to the polymerization of G-actin into F-actin[10]. Lysophosphatidic acid (LPA) stimulation of cells, known to activate Rho-GTPases[11], induces F-actin polymerization involving Rho-kinase (ROCK), LIM kinase and cofilin[11–13]. This depletion of G-actin stimulates the translocation of cytoplasmic MAL protein into the nucleus, where MAL dimers cooperate with SRF to stimulate transcription[13]. One SRF target gene is *Actb* (encoding β-actin) itself, whose activation, and the resulting rise in cytoplasmic G-actin, may participate in turning off of SRF-directed transcription by sequestering MAL back into the cytoplasm[13]. Other SRF target genes regulating cytoskeletal dynamics are *Vcl*, *Zyx*, *Itgb1* and *Gsn*[8,14], the last encoding actin-severing activity.

The function of SRF in neurons[15] was only explored recently using conditional deletion of *Srf* in the brain. In the adult brain, IEG induction and synaptic plasticity are impaired by SRF deficiency[16]. Also, conditional prenatal *Srf* deletion results in impaired neuronal migration of the rostral migratory stream[17]. Here we show that in the hippocampi of SRF-deficient mouse forebrains, mossy fibers did not segregate into two anatomically distinct bundles; instead, they preferentially grew between CA3 pyramidal neurons, where they aberrantly synapsed onto CA3 somata. This pathfinding defect was associated with decreased neurite outgrowth and a reduction in ephrin-A– and semaphorin-mediated axonal repulsion *in vitro*. Rho-GTPases required SRF activity to fulfil their function in growth cone guidance. MAL represents a new link neurons conferring Rho-GTPase signaling to SRF activation and *Actb* dynamics.

RESULTS

SRF deficiency results in early embryonic death (embryonic day (E) 6.5; ref. 18) in mice. Therefore, we used conditional, forebrain-specific *Srf*-null mutagenesis by crossing mice bearing a *loxP*-flanked ('floxed') *Srf* allele (*Srf-flex1neo*; ref. 19) with a strain driven by the calcium/calmodulin–dependent protein kinase II (CamKIIα) promoter and expressing Cre recombinase[17,20]. Cre-mediated *Srf* deletion in neurons

[1]Interfakultäres Institut für Zellbiologie, Abt. Molekularbiologie, Eberhard-Karls-Universität Tübingen, Auf der Morgenstelle 15, 72076 Tübingen, Germany. [2]Institut für Anatomie und Zellbiologie, Albert-Ludwigs-Universität Freiburg, 79104 Freiburg, Germany. [3]Deutsches Krebsforschungszentrum (DKFZ), Molekularbiologie der Zelle I, Heidelberg, Germany. Correspondence should be addressed to A.N. (alfred.nordheim@uni-tuebingen.de).

Received 4 November 2005; accepted 8 December 2005; published online 15 January 2006; doi:10.1038/nn1627

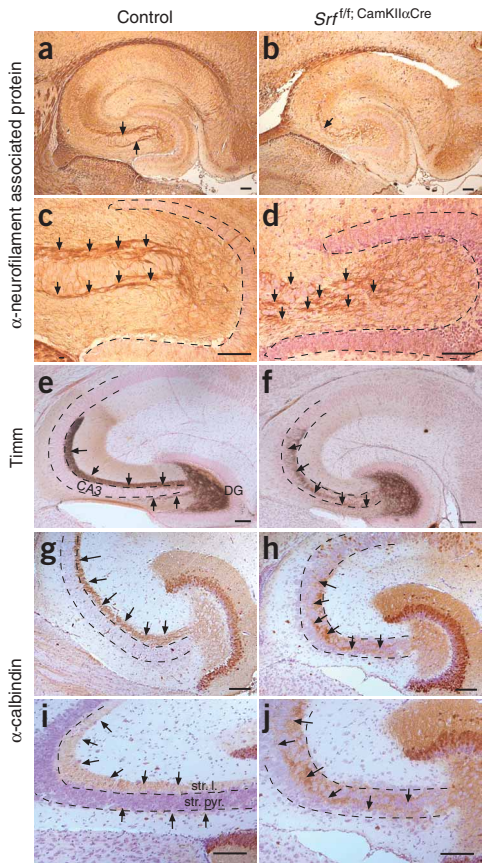

Figure 1 *Srf* mutants show hippocampal neurite loss and mossy fiber misrouting *in vivo*. (**a**–**d**) In control mice (**a**,**c**), mossy fibers emanating from the DG (dotted lines) bifurcated into the supra- and infrapyramidal branches (arrows). SRF-deficient neurites (**b**,**d**) left the DG in a dispersed fashion (arrows) without any of the bifurcation that was typically seen for control neurites (**a**,**c**). (**e**,**f**) Timm staining exclusively stained the trajectories of mossy fibers. Mossy fibers of control mice (arrows in **e**) bifurcated and navigated precisely along the borders of the CA3 region (dotted lines). In contrast, fibers lacking SRF (arrows in **f**) did not split and instead grew preferentially along CA3 pyramidal cell somata. (**g**–**j**) Calbindin staining labeled DG cell bodies and their extensions. When compared to wild-type controls (**g**,**i**), SRF-deficient nerve terminals (**h**,**j**) were strongly misrouted, with virtually all nerve fibers (arrows) growing inside the stratum pyramidale rather than outside (in the stratum lucidum). str. l., stratum lucidum; str. pyr., stratum pyramidale. Scale bar, 100 μm.

started just before birth and was largely restricted to forebrain areas[17]. SRF-deficient offspring could be easily distinguished from wild-type litters by their severe motor dysfunctions, including a loss of balance and ataxic movements. *Srf* $^{f/f;\ CamKII\alpha Cre}$ mice died between postnatal days (P) 17 and 20 (ref. 17).

In the hippocampus, *Srf* mRNA was localized to the hippocampal anlage at E17, and expression in the DG and cornu ammonis (CA) regions lasted into adulthood (**Supplementary Fig. 1** online; refs. 16 and 17). Reduction of *Srf* mRNA (**Supplementary Fig. 1**) and SRF protein[16,17] in *Srf* mutants was observed in the DG and CA regions.

SRF controls mossy fiber circuit assembly *in vivo*

We first asked whether the assembly of hippocampal circuits was affected in *Srf* mutants. We used immunohistochemical stainings between P14 and P16, which represent timepoints well suited for the analysis of hippocampal development that, for the most part, takes place postnatally.

Visualization of nerve fibers with an antiserum to neurofilament-associated protein (α-NFAP) revealed notable differences in the mossy fiber projection (**Fig. 1a–d**). In the wild type, mossy fibers emanating from the DG bifurcated and precisely navigated on either side of CA3 pyramidal neurons (arrows **Figs. 1a,c**; $n = 5$, 100% penetrance). This segregation of mossy fibers into supra- and infrapyramidal tracts was abolished in *Srf* mutants (**Fig. 1b,d**). Timm staining to selectively label the mossy fibers also revealed the absence of mossy fiber bifurcation in

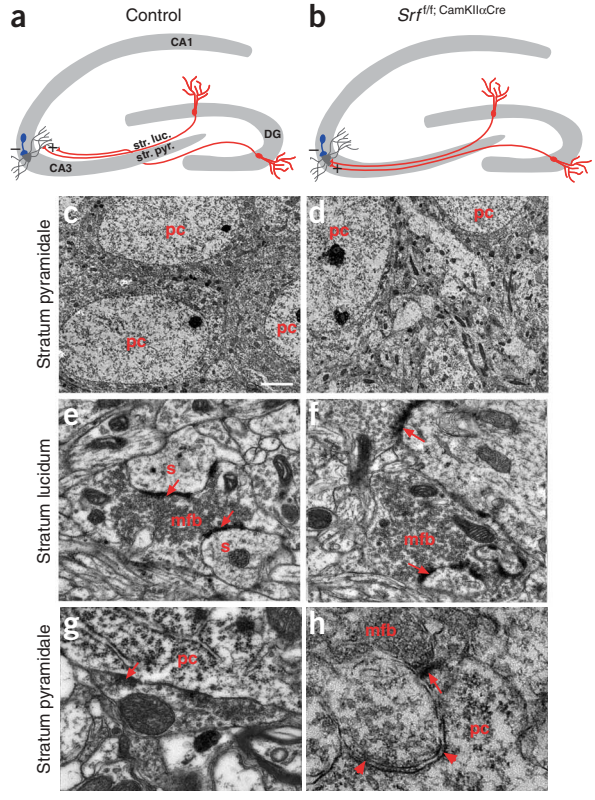

Figure 2 Aberrant synaptic targeting of SRF-deficient mossy fiber terminals. (**a**,**b**) Schematic of axonal misrouting and aberrant synaptic targeting in mossy fibers in *Srf* mutant mice (**b**), as compared to those in control mice (**a**). Blue, inhibitory (–) interneurons establishing symmetric synapses with CA3 pyramidal neurons. Red, excitatory (+) asymmetrical mossy fiber synapses. (**c**) Electron microscopical images in P14 control mice with densely packed CA3 pyramidal cells and only small intercellular spaces between pyramidal cell bodies. (**d**) Enlarged intercellular spaces between CA3 pyramidal cells were frequently observed in *Srf* mutants. (**e**) A characteristic mossy fiber bouton in stratum lucidum terminating on dendritic spines originating from the apical dendrite of a CA3 pyramidal cell in a control mouse (arrows). (**f**) *Srf* mutant mossy fibers barely formed synapses with apical dendrites in the stratum lucidum. (**g**) Inhibitory symmetrical synapses were typically formed between interneurons and the cell bodies of CA3 pyramidal neurons. (**h**) The majority of mossy fiber synapses (mfb, arrow) of *Srf* mutants were aberrantly formed in the stratum pyramidale with CA3 somata. These mossy fiber synapses (arrow) were asymmetric (excitatory) and were found next to the normal symmetric (inhibitory) synapses (arrowheads). mfb, mossy fiber bouton; pc, pyramidal cell; s, spine; str. luc., stratum lucidum; str. pyr., stratum pyramidale. Scale bars: 5 μm in **c**, 4 μm in **d**, 0.8 μm in **e**, 0.5 μm in **f**, 0.3 μm in **g** and 0.2 μm in **h**.

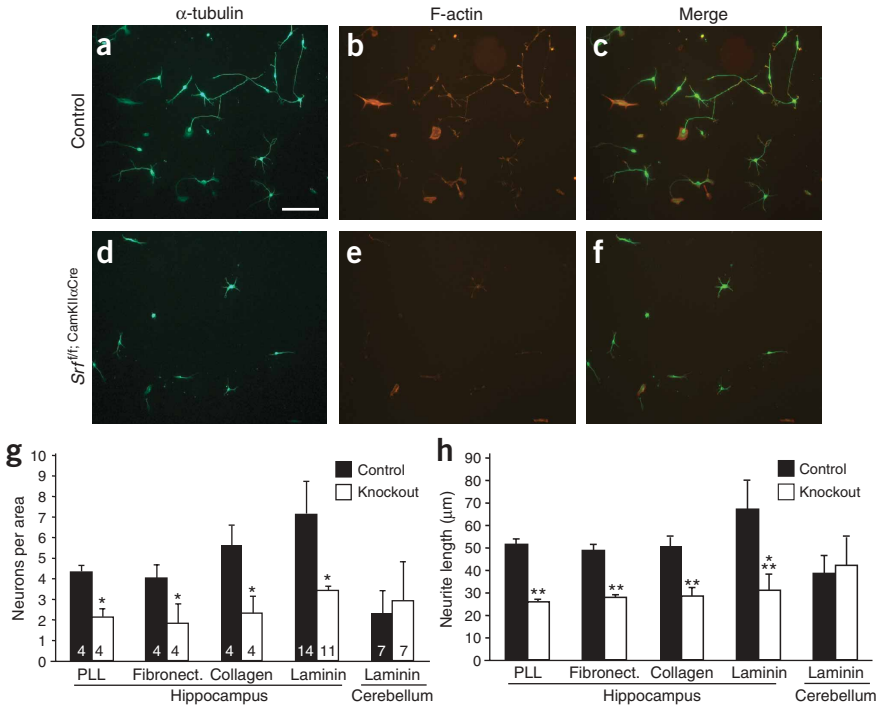

Figure 3 *Srf* mutants show impaired neurite outgrowth. (**a**–**h**) Hippocampal neurons derived from control pups (**a**–**c**) and *Srf* mutant littermates (**d**–**f**) were grown on laminin. *Srf* mutant neurons differed from wild-type neurons in at least two ways: first, the number of neurons with neurite outgrowth was reduced (see **g**); second, neurite length of those mutant neurons showing growth was decreased, regardless of the outgrowth-promoting substrate tested (**h**). Notably, Cre-negative cerebellar neurons derived from *Srf* mutant mice behaved similarly to those derived from controls (**g**,**h**). F-actin staining was generally fainter in mutant neurons (see also **Supplementary Fig. 4**). Fibronect., fibronectin; PLL, poly-L-lysine. Scale-bar, 100 μm. Numbers inside histogram bars represent the number of animals tested.

Srf mutants. Instead of bifurcating, *Srf*-null mossy fibers preferentially grew on and between CA3 pyramidal somata in the stratum pyramidale, rather than outside in the stratum lucidum (**Figs. 1e**,**f**; $n = 3$, 100% penetrance). Calbindin staining (**Fig. 1 g**–**j**) highlighted mossy fiber trajectories and the localization of granule-cell bodies. Similar to the results seen with α-NFAP and Timm staining, calbindin-positive, SRF-deficient mossy fibers navigated inside the stratum pyramidale (**Figs. 1h**,**j**; $n = 3$, 100% penetrance).

Overall, the number of neurons and the layering in the mutant DG appeared unaltered, except for the subgranular zone (as judged by Prox1 and doublecortin immunostaining; data not shown).

Aberrant synapse formation in *Srf* mutants

The abnormality in mossy fiber guidance (**Fig. 1** and **Fig. 2a**,**b**) led us to explore the synaptic fate of misrouted mossy fiber terminals (**Fig. 2**). In wild-type mice, mossy fibers establish asymmetric excitatory synapses with apical dendrites of CA3 pyramidal neurons in the stratum lucidum. Additionally, CA3 somata received inhibitory input by means of symmetric synapses formed with interneurons in the stratum pyramidale (**Fig. 2a**,**b**).

Electron microscopy (EM) revealed that the somata forming the stratum pyramidale were densely packed in wild-type mice, with little space between individual CA3 cells (**Fig. 2c**). In contrast, in *Srf* mutants (**Fig. 2d**) this intercellular space was enlarged and filled with mossy fiber terminals, in keeping with the misrouting outlined above (**Fig. 1**). In the stratum lucidum, wild-type mossy fiber terminals elaborated boutons exclusively on the spines of apical CA3 dendrites (**Fig. 2e**). In contrast, in *Srf* mutants ($n = 3$; 100% penetrance), few mossy fiber boutons were found in the stratum lucidum (**Fig. 2f**). In the stratum pyramidale of wild-type mice (**Fig. 2g**), we found (mean ± s.d.) 6.3 ± 1.7 symmetrical synapses per 10 μm^3 and no asymmetrical synapses. In *Srf* mutants (**Fig. 2h**), the number of symmetrical synapses at the CA3 somata was comparable to that in the wild type (6.7 ± 1.4), but additionally we saw 2.3 ± 0.8 asymmetrical synapses—that is, one-fourth of the contacts at CA3 pyramidal cell somata belonged to misplaced mossy fiber terminals. Mossy fiber terminals in the CA3 region were identified by immuno-EM with antibodies to the synaptic vesicle protein synaptoporin[21], also known as synaptophysin II (**Supplementary Fig. 2** online).

In sum, SRF-deficient mossy fiber terminals were able to form postsynaptic densities, which—incorrectly—localized to CA3 somata and somatic spine-like protrusions, instead of localizing to apical dendrites.

SRF stimulates neurite outgrowth *in vitro*

Inspection of mossy fiber projection indicated decreased axonal length in *Srf* mutants (compare **Fig. 1c**,**d**). Therefore, we used *in vitro* neurite outgrowth assays to investigate a potential function of SRF in neurite extension. The results we obtained largely reflected the situation for the mossy fiber pathway, as more than 80% of the cultured neurons expressed the granule-cell marker Prox1 (data not shown).

Neurons from wild-type mice gave rise to long and well-elaborated neurites (**Fig. 3a**–**c**). *Srf* mutant neurons (**Fig. 3d**–**f**), in contrast, consistently revealed reduced numbers of neurons with outgrowth, regardless of the substrate (**Fig. 3g**; $P = 0.013$, poly-L-lysine; $P = 0.033$, fibronectin; $P = 0.025$, collagen; $P = 0.045$, laminin). Also, *Srf* mutant neurites were significantly shorter than those of the wild type, indicating that SRF is involved in promoting neurite outgrowth (**Fig. 3h**; $P = 0.0013$, poly-L-lysine; $P = 0.0012$, fibronectin; $P = 0.0012$, collagen; $P = 0.00054$, laminin). SRF-expressing cerebellar neurons of *Srf* $^{f/f;\ CamKII\alpha Cre}$ mice (**Supplementary Fig. 1**), which are essentially devoid of Cre recombinase activity, were not disturbed.

We further investigated the morphology of *Srf* mutant neurons and noticed a more rounded appearance, which suggested that SRF may contribute to neuronal polarization (**Fig. 3d**; **Supplementary Fig. 3** online). Indeed, the ratio of the longest neurite to the average length of the surrounding minor neurites was reduced in *Srf* mutant neurons (4.74 ± 0.9, wild type; 2.22 ± 0.3, mutants; $n = 5$; $P = 0.003$). The overall number of neurites on individual neurons was not substantially altered (data not shown). Using terminal deoxynucleotidyl transferase-mediated deoxyuridine triphosphate nick end-labeling (TUNEL) assays and staining for activated caspase-3, we did not observe elevated levels of apoptosis in *Srf* mutant cultures (data not shown).

As described above, the loss of SRF was accompanied by decreased neurite outgrowth. We complemented these findings by replenishing *Srf* mutant neurons with a constitutively active SRF derivative

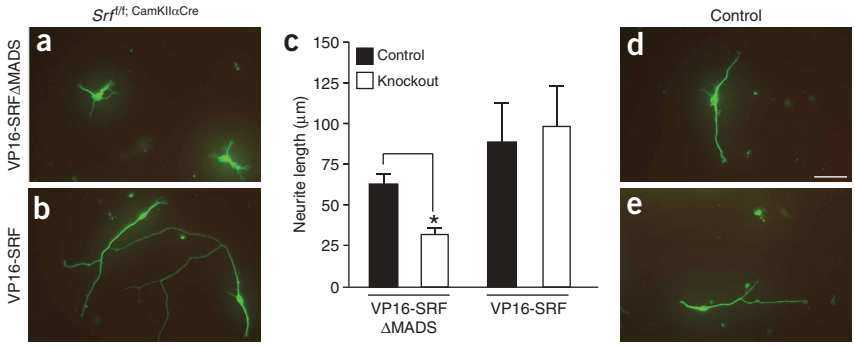

Figure 4 Overexpression of SRF-VP16 promotes neurite elongation. (**a**–**e**) SRF-deficient (**a**) and control neurons (**d**) were electroporated to express an inactive SRF control construct (SRF-VP16ΔMADS) missing the DNA binding domain. As expected, electroporated neurons of wild-type littermates still grew neurites that were twice the length of those in *Srf* mutant neurons (see **c** and **Fig. 3**). (**b**,**e**) Replenishing *Srf* mutant neurons (**b**) with constitutively active SRF (SRF-VP16) stimulated a marked increase in neurite length. In control neurons (**e**), additional neurite length was also achieved by SRF-VP16, albeit to a lesser extent than in mutants. (**c**) Control neurites expressing SRF-VP16ΔMADS grew twice as long as the *Srf* mutant neurites (61 ± 8.5 μm versus 31.3 ± 3.7 μm). SRF-VP16 enhanced neurite length markedly in neurons lacking endogenous SRF protein (96.1 ± 29 μm). Scale bar, 25 μm.

(SRF-VP16). The overexpression of SRF-VP16 in *Srf* mutant neurons stimulated a more than threefold (306 ± 76%) increase in neurite length compared to *Srf* mutant neurons expressing SRF-VP16ΔMADS protein, which is nuclear but incapable of binding DNA (**Fig. 4a–c**; ref. 8). SRF-VP16 had only a weak effect on neurite outgrowth in wild-type neurons with endogenous SRF docking at promoter sites (**Fig. 4d,e**). The length of neurites in neurons expressing SRF-VP16ΔMADS was indistinguishable from that in control vector–electroporated neurons (data not shown).

Srf mutant neurons showed decreased expression of the SRF target gene *Actin* (**Fig. 3e**; **Supplementary Fig. 4** online). The remaining actin polymers, however, were still properly concentrated at the growth cones and the cell body (**Supplementary Fig. 4**). Thus, we assessed whether decreased actin levels alone were affecting neurite outgrowth and guidance in *Srf* mutants. We found that the expression of full-length β-actin in neurons led to only slight increases in neurite length and growth cone collapse rate in both *Srf* mutant neurons and wild-type neurons (**Supplementary Fig. 4**).

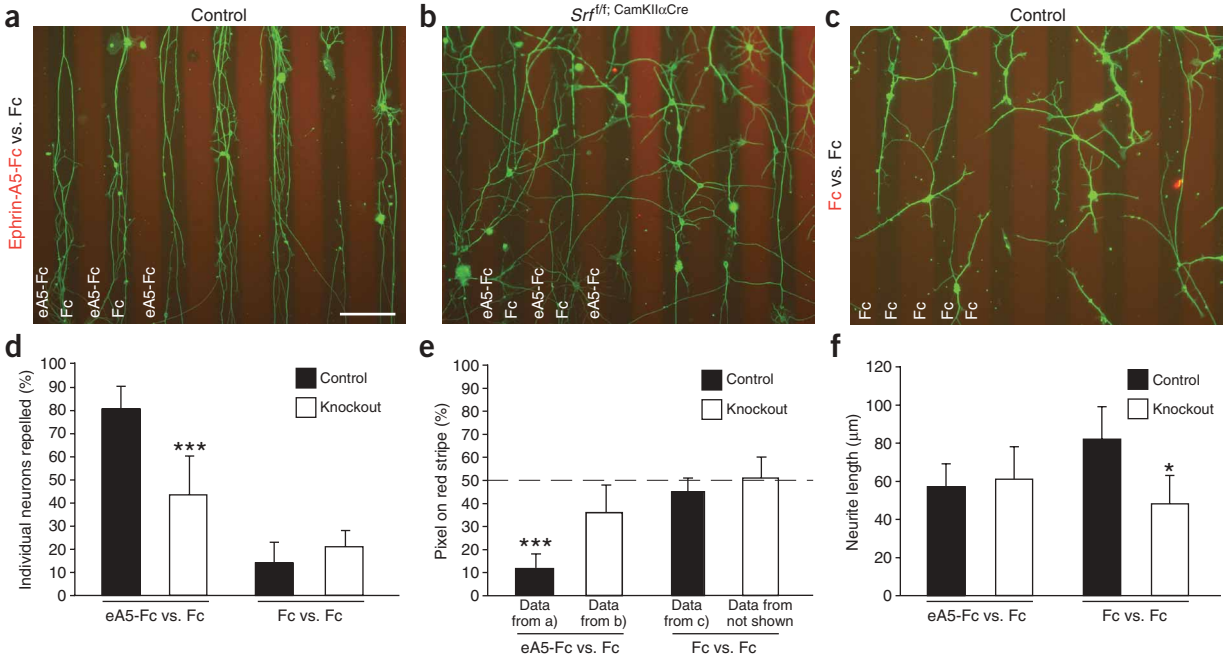

Figure 5 SRF is required for contact-mediated, repulsive axon guidance *in vitro*. (**a**) Hippocampal neurons derived from control littermates were grown on alternating stripes containing ephrin-A5–Fc (eA5-Fc, red stripes) or control protein (Fc, dark stripes). Typically, EphA receptor–expressing neurites were strongly repelled upon interacting with ephrin-A5. (**b**) SRF-deficient neurons were less sensitive toward the repulsive activity of ephrin-A5; hence more neurites crossed the ephrin-A5–containing stripes. (**c**) Control experiments with all stripes containing Fc protein (Fc versus Fc) showed random outgrowth of neurites on these carpets. (**d**) In experiments using ephrin-A5 stripes (as shown in **a**), 80.6 ± 12.7% of control neurites were repelled. In contrast, only 44 ± 17% of SRF-deficient neurites were sensitive to ephrin-A5. On control-stripe carpets (Fc versus Fc), as expected, only a few neurites were repelled, independent of genotype. (**e**) Only 12 ± 6% of pixels (representing neurites) from control neurons were not repelled by ephrin-A5; a threefold increase (36 ± 12% s.d.) was observed for *Srf* mutant neurons. Theoretically, a 50% chance exists for any given pixel to localize on either stripe. This was indeed observed for control stripes (Fc versus Fc). (**f**) SRF-containing neurites still grew almost twice as long as neurons lacking SRF (82 ± 17 μm for controls versus 48 ± 5 μm for mutants) on control stripes (see **c**). In experiments with ephrin-A5 stripes, control neurites grew slightly less, whereas (less sensitive) SRF-deficient neurons showed a subtle increase in neurite length. Scale bar, 100 μm.

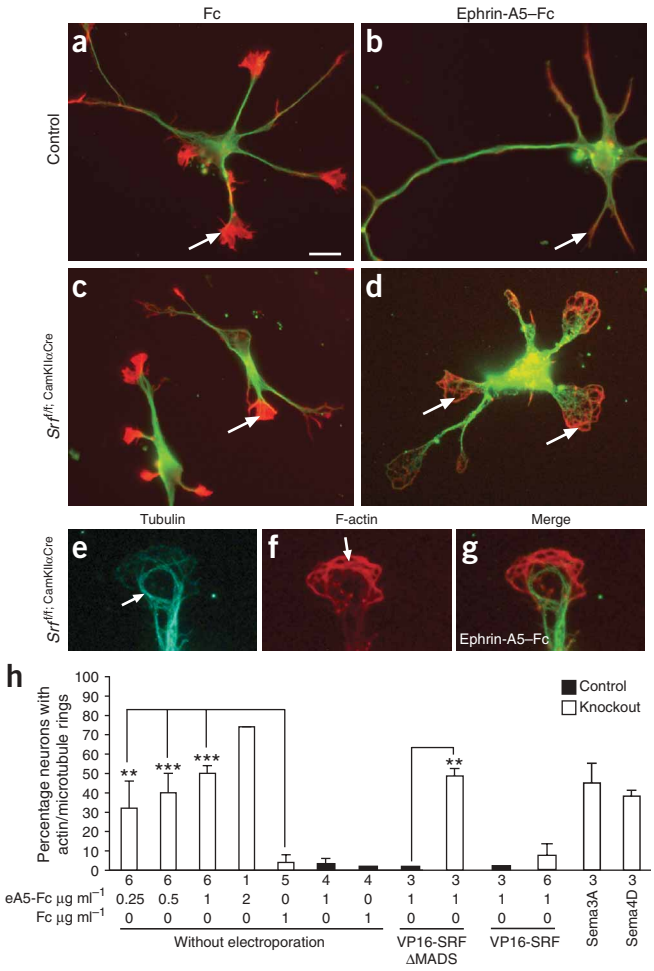

Figure 6 Growth cone dynamics are severely impaired in *Srf* mutants. (**a**,**b**) In the presence of control protein (Fc), SRF-containing control neurons bore well-elaborated growth cones (arrow in **a**) with filopodial and lamellipodial structures, as revealed by staining for F-actin (red). Bath application of ephrin-A5 (**b**) and semaphorins (not shown) triggered the breakdown of the actin cytoskeleton, resulting in complete growth cone collapse (arrow in **b**). (**c**–**h**) Growth cones in *Srf* mutants, before the induction of collapse (**c**), appeared as well defined as those in the controls (see **a**). Incubation with ephrin-A5 (**d**) and semaphorins (see **h**) induced new ring-like structures (arrows) at the growth cones, rather than generating complete collapse. These ring-shaped structures consisted of both F-actin (red) and microtubules (green). (**e**–**g**) Higher magnifications of results in **d**. (**h**) Quantification of neurons bearing at least one F-actin–microtubule ring after ephrin-A5 or semaphorin induction. The percentage of SRF-deficient neurons bearing these ring-shaped structures increased for ephrin-A5 in a dose-dependent manner. These rings were almost completely absent in mutant neurons incubated with control protein (Fc) and in wild-type neurons treated with either ephrin-A5 or control protein. Overexpression of SRF-VP16 in SRF-deficient neurons profoundly interfered with the growth of F-actin–microtubule rings and allowed for complete growth cone collapse. Note that for the sake of visualization of mutant growth cones, exposure times were increased two- to threefold over control exposures. Scale bar, 10 μm. Numbers beneath histogram bars represent the numbers of mice tested.

Overall, our loss-of-function and gain-of-function experiments clearly point toward an important function of SRF in promoting neurite outgrowth *in vitro* (**Figs. 3** and **4**) and in *vivo* (**Fig. 1**).

Hippocampal neurons require SRF for axonal repulsion

The loss of accurate mossy fiber guidance (**Fig. 1**) encouraged us to investigate whether axon guidance molecules depend upon SRF-directed transcription. One family of guidance molecules leading to contact-mediated repulsion of growth cones are the ephrins[22]. Ephrin-As in the environment activate EphA receptors expressed on, for instance, hippocampal neurites[23]. Ephrin-As have predominantly inhibitory effects on hippocampal neurons[23,24] although, depending on (for instance) the concentration used, they can either stimulate or inhibit neurite outgrowth[25].

Using the stripe assay, we asked whether EphA-mediated repulsion was dependent on SRF (**Fig. 5**). In these experiments, we arranged carpets of alternating stripes consisting of purified ephrin-A5–Fc and control protein (Fc). This version of the assay measured the activity of an individual repulsive molecule; thus extrapolations to the complex environment met by axons *in vivo* have to be made cautiously.

Typically, most wild-type hippocampal neurites (**Fig. 5a**) were strongly repelled from entering ephrin-A–containing stripes; thus, they preferentially grew on the control stripes (80.6 ± 9.9%; $n = 14$). Similarly, when calculating the number of green pixels (representing neurites) localized on ephrin-A-containing red stripes, only 12% (12.1 ± 6.6%; $n = 11$) were not repelled. When *Srf* mutant neurons (**Fig. 5b**) were challenged to distinguish between ephrin-A5–Fc and Fc stripes, a two to threefold reduction in the number of the neurites repelled by ephrin-A5 was noticed (44 ± 17%, $P = 2.1 \times 10^{-4}$ for individual neurons; 35.1 ± 15.5%, $P = 5 \times 10^{-10}$ for ImagePro; $n = 8$).

Using stripe assays consisting of control protein only (Fc versus Fc), neurites of both genotypes grew out in a random fashion (**Fig. 5c**,**d**; 14 ± 9% for wild-type neurons; 21 ± 7% for mutants; $n > 5$). ImagePro analysis (**Fig. 5e**) revealed a random distribution of pixels over the carpet, in keeping with a theoretical 50% chance of the neurites localizing on either stripe (43 ± 7% for wild-type neurons; 52.9 ± 9.8% for mutants; $n > 3$).

Additionally, we noticed that mutant neurites were insensitive to the repulsive effect of ephrin-A5 on neurite outgrowth (**Fig. 5f**). It is likely that ephrin-A5 presented a growth stop signal at stripe boundaries for the wild-type neurites but not for SRF-deficient neurites. At the same time, on carpets containing Fc (+ laminin) only, wild-type neurons still grew to twice the length of *Srf* mutants (82 ± 17 μm for the wild type versus 48 ± 5 μm for mutants; $n = 5$).

Impaired cytoskeletal dynamics in *Srf* mutant growth cones

Dynamic changes in the polymerization of cytoskeletal filaments are critical for steering growth cones toward their targets[26]. The local induction of growth cone collapse by repulsive guidance cues such as ephrin-As triggers the depolymerization of F-actin. Because of SRF's ability to adjust cytoplasmic actin abundance, we investigated a possible function of SRF in growth cone collapse (**Fig. 6**).

Typically, control growth cones in the presence of Fc alone were well elaborated, with multiple filopodia and lamellipodia (**Fig. 6a**). Bath application of ephrin-A5 resulted in the collapse of growth cones, as evidenced by an almost complete breakdown of F-actin (**Fig. 6b**). After bath application of the control protein, growth cones in the *Srf* mutants had a structure similar to that in the wild-type cells, although we noted a generally more rounded appearance (**Fig. 6c**). Remarkably, ephrin-A5 treatment of SRF-deficient neurons, instead of inducing complete collapse as seen for wild-type neurons (**Fig. 6b**), resulted in the formation of unusual ring-shaped fibers consisting of F-actin and, notably, also of microtubules (**Figs. 6d–g**). These previously undescribed ring-shaped structures were almost completely absent in wild-type neurons incubated with either Fc or ephrin-A5–Fc and in

mutants incubated with Fc alone (**Fig. 6h**). The capability for full growth cone collapse in *Srf* mutants could be restored by the introduction of SRF-VP16, but not by of SRF-VP16ΔMADS (**Fig. 6h**).

To investigate whether the appearance of these ring-shaped structures was specific to ephrins or could be similarly stimulated by other guidance cues, we induced growth cone collapse with semaphorin 3A and 4D (**Fig. 6h**). Semaphorins elicit hippocampal growth cone collapse[27,28]. Similar to ephrin-As, semaphorins caused the formation of F-actin–microtubule rings in SRF-deficient neurons, albeit to a lesser extent (as a percentage of neurons with actin-microtubule rings: Sema3A, 47.6 ± 14.3%; Sema4D, 38.3 ± 4.1%; $n = 3$).

Altogether, growth cone collapse was markedly impaired in *Srf* mutants. This was in keeping with the insensitivity of *Srf* mutant neurites to guidance molecules, as observed in the stripe assay (**Fig. 5**).

SRF is required for Rho-GTPase signaling in neurons

It is believed that the Rho-GTPases Rac1 and Cdc42 are positive regulators of neurite outgrowth whereas RhoA is a negative regulator, although exceptions have been reported[29]. We used hippocampal neurons to ask whether Rac1- and Cdc42-mediated neurite elongation and RhoA-mediated inhibition of neurite outgrowth were dependent on SRF (**Fig. 7a**,**b**). We expressed constitutively active variants—RhoA-V14, Cdc42-V12 and Rac1-V12—in wild-type and SRF-deficient neurons (**Fig. 7**; data for Cdc42 not shown).

In line with previous reports[30], Rac1 and Cdc42, as compared to vector controls, increased the neurite length of wild-type neurons by 38.3 ± 4% and 41 ± 4.3%, respectively ($n = 3$; **Fig. 7a**,**b** and data not shown). In contrast, in agreement with other studies[30,31], RhoA-V14 decreased wild-type neurite length (**Fig. 7a**,**b**) by 32.7 ± 1.1% ($n = 3$; $P = 0.0065$).

Notably, neither of these Rho-GTPases was able to exert its function without SRF (**Figs. 7a**,**b** and data not shown). RhoA-, Rac1- and Cdc42-expressing *Srf* mutant neurons had neurites with indistinguishable, albeit reduced, lengths ($n = 3$; $P = 0.012$, control; $P = 0.012$, Rac1; $P = 0.0065$, RhoA; $P = 0.03$, Cdc42).

MAL and SRF cooperate to regulate actin dynamics

Dimers of nuclear MAL cooperate with SRF to stimulate transcription[13], and a cytoplasm-to-nucleus translocation of MAL has been shown in cortical neurons[32]. Here we provide evidence that MAL can influence neurite outgrowth and the growth cone collapse of neurons and that it thereby relies on SRF activity (**Fig. 7c–e**).

MAL variants lacking the C-terminal transactivation domain (MAL C471 and MAL ΔNC471) clearly behaved in a dominant-negative

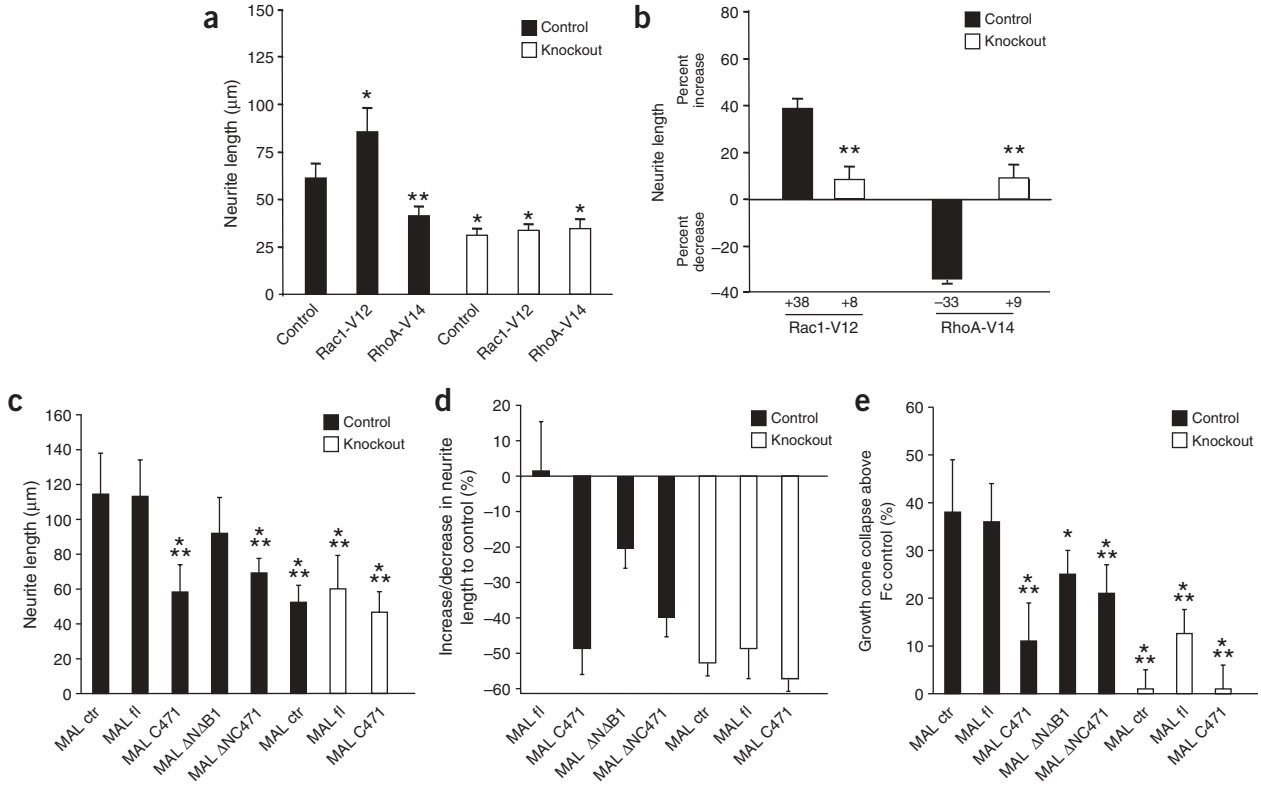

Figure 7 Rho-GTPase activity and the function of the SRF cofactor MAL in hippocampal neurons. (**a**,**b**) Effect of Rho-GTPases on neurite length derived from wild-type mice and *Srf* mutants. Quantification of the absolute neurite length (**a**) and relative changes (**b**) to control vector–transfected neurons are indicated. In relation to the average neurite length obtained in control vector–electroporated wild-type neurons, constitutively active Rac1-V12 stimulated a 38.3 ± 4% increase in neurite length. In contrast, RhoA-V14 reduced neurite length in control neurons by 32.7 ± 1.1%. *Srf*-null neurons electroporated with a control vector Rac1-V12 or RhoA-V14 only grew short neurites, thus demonstrating that neurite elongation and stalling, respectively, require SRF activity in the nucleus. (**c**,**d**) Interfering with the function of the SRF cofactor MAL through the expression of multiple dominant-negative MAL variants (MAL C471, MAL ΔNΔB1 and MAL ΔNC471) reduced neurite length in control neurons. Full-length MAL could not rescue neurite outgrowth in *Srf* mutants. In **d**, the MAL control construct MAL ΔNΔB1ΔLZ (MAL control) was used as baseline to indicate relative changes in neurite outgrowth. (**e**) The percentage increase of growth cone collapse above that in Fc controls. In the presence of control (MAL ΔNΔB1ΔLZ) and full-length MAL, control neurons showed a robust growth cone collapse response. However, this was blocked to a significant degree by targeting MAL with various dominant-negative constructs.

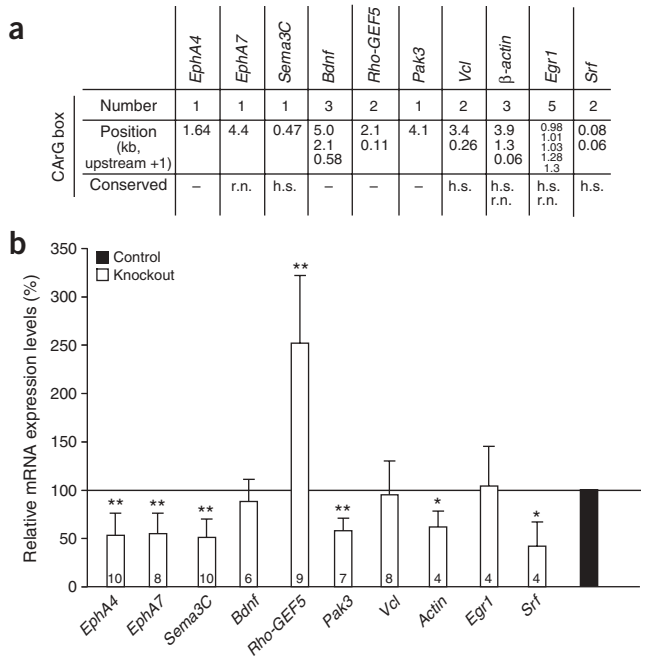

Figure 8 Identification of putative *Srf* target genes in hippocampal neurons. (**a**) Table depicting number, position (relative to transcriptional start sites) and species conservation (mouse versus human and/or rat) of CArG boxes in promoters of potential *Srf* target genes. CArG boxes found up to 5 kb upstream of the +1 transcriptional start position are included. (**b**) RNA expression of potential *Srf* target genes listed in **a**. Relative changes in RNA levels of control versus SRF-deficient hippocampal cell cultures as assessed by RT-PCR. RNA amounts obtained for control mice were set to 100%. Digits inside bars indicate the numbers of both mutant and control mice investigated for any given gene. Levels of *Srf* RNA in SRF-deficient neurons dropped to ~40% of that in control neurons, and RNA abundance for *Actin*, a well-established SRF target gene, was decreased by 40% on average. These two values can be used as a baseline to evaluate the obtained expression differences. h.s., *Homo sapiens*; r.n., *Rattus norvegicus*.

manner and interfered with neurite outgrowth in wild-type neurons (**Fig. 7c**,**d**; MAL C471 = 58.3 ± 15.6 µm; MAL ΔNC471 = 69.2 ± 16.8 µm; n = 8 and 6, respectively). Another MAL mutant (MAL ΔNΔB1) that can act in a dominant-negative manner had a less pronounced, although reproducible, negative effect on neurite extension (91.9 ± 41.1 µm; n = 6). As a control ('MAL control'), we used a MAL construct (MAL ΔNΔB1ΔLZ) lacking the N terminus (responsible for actin association and Rho regulation), the B1 domain (involved in nuclear import) and—notably—the LZ region (responsible for dimerization)[13]. Overexpression of full-length MAL (MAL fl) in wild-type neurons did not alter neurite outgrowth (114.3 ± 23.6 µm, MAL control; 112.3 ± 23.7 µm, MAL fl; n = 12 and 8, respectively). In initial experiments, MAL ΔNΔB1ΔLZ resulted in approximately the same neurite length as that seen with GFP- or mock-electroporated neurons (data not shown). We tested the localization of all MAL constructs used; these were as previously reported (ref. 13 and data not shown). In *Srf* mutant neurons, none of the MAL constructs was capable of modulating neurite length either positively or negatively (**Fig. 7c**,**d**).

We next asked whether MAL was able to interfere with ephrin-A5–mediated growth cone collapse (**Fig. 7e**). Here, full-length MAL and MAL ΔNΔB1ΔLZ permitted complete ephrin-A5–induced growth cone collapse in wild-type neurons (36 ± 12% and 38 ± 9%, respectively). In contrast, all dominant-negative MAL constructs strongly impeded this reaction (**Fig. 7e**; 11 ± 4.8%, 25 ± 10% and 21 ± 7% for MAL C471, MAL ΔNΔB1 and MAL ΔNC471, respectively). As with neurite outgrowth, none of the MAL constructs could rescue full growth cone collapse in *Srf* mutants, indicating that MAL and SRF are intrinsic partners in mediating transcription.

Identification of new putative SRF target genes

To identify potential new neuronal SRF target genes, we screened 120–150 well-known candidate genes for the presence of CArG boxes (SRF binding sites) within 5 kilobase (kb) upstream of their transcriptional start sites (**Fig. 8a**). Subsequently, we measured mRNA expression by quantitative real-time polymerase chain reaction (RT-PCR) to compare wild-type and SRF-deficient hippocampal cell cultures.

To estimate the maximum mRNA downregulation attainable in our cultures, we analyzed the SRF target gene *Actin* and *Srf* itself. *Actin* and *Srf* levels in *Srf* mutants were reduced to 62.3 ± 16.6% (n numbers in bars; P = 0.019) and 41.5 ± 25% (P = 0.021), respectively, of those in control mice. The presence of Cre recombinase–negative glia cells (approximately 20% as judged by staining with glial fibrillary acid protein, GFAP) in our cultures caused an underestimation of the SRF-dependent changes in neuronal RNA levels. *Vcl* and *Egr1*, well-known SRF target genes, were not affected in primary hippocampal neurons but had decreased expression in P16 hippocampi (77 ± 8% of control values, n = 6, P = 0.007; and 69.2 ± 0.7% of control values, n = 3, P = 0.011; data not shown).

With regard to genes encoding axon guidance molecules, we show only those genes for which the CArG boxes were localized in the respective promoters (**Fig. 8a**) and changes in mRNA levels were consistently detected (**Fig. 8b**). Among the Eph receptor genes, we found that *Epha4* and *Epha7* contained CArG boxes. The overall protein expression of all EphA receptors localized on hippocampal neurons (that is, EphA3 to EphA7; ref. 33) appeared unaltered, as judged by ephrin-A5–Fc staining on cultures and ephrin-A5–alkaline phosphatase (ephrin-A5–AP) staining on sections (data not shown). Nevertheless, levels of RNA for individual receptors—namely, *Epha4* and *Epha7* RNAs—were reduced to 52.9 ± 23% and 55.3 ± 21% of controls.

Within the family of semaphorins, only *Sema3c* mRNA levels reproducibly dropped to 50.6 ± 19.7% (P = 0.004) those of controls. *Bdnf*, in contrast, although equipped with three CArG boxes (**Fig. 8a**), was not changed in *Srf* mutant cells and P16 hippocampi (data not shown). When we examined possible signaling components that convey receptor activity from the neuronal surface to the nucleus, we found that the expression of *Rho-GEF5* and the Rac1 effector *Pak3* were significantly altered by SRF deficiency. RNA levels for *Rho-GEF5* were upregulated two and a half times (to 252.2 ± 79%; P = 0.0011) compared to wild-type neurons, whereas *Pak3* was downregulated by approximately 40% (to 58.3 ± 13.8%; P = 0.0013).

In summary, here we identified several putative new SRF target genes that encode guidance receptors, ligands and signaling intermediates, with intimate links to processes of neurite outgrowth, guidance and synaptic targeting.

DISCUSSION

The assembly of neuronal circuits requires coordinated neurite outgrowth, axon guidance and synapse formation. We uncovered a crucial function of the transcription factor SRF in each of these three mechanisms of neuronal network formation.

Mossy fibers emanating from the DG in *Srf* mutants were shortened *in vivo* (**Fig. 1**), demonstrating, together with *in vitro* experiments

(**Figs. 3** and **4**), an important contribution of SRF toward promoting neurite outgrowth. The reduction in neurite outgrowth associated with SRF deficiency might be the consequence of impairments in either substrate adhesion or budding and extension of neurites, or it might be be linked to increased apoptosis. TUNEL assays and staining for active caspase-3 ruled out increased apoptosis as the cause for decreased neurite outgrowth, in agreement with previous reports[16,17]. In contrast, decreased cell adhesion, spreading and migration, together with impaired cytoskeletal and focal adhesion dynamics, were previously reported in *Srf* mutant cells[8,17]. Neurite outgrowth is closely related to these processes; thus, it is likely that SRF-directed mechanisms operating in ES cells similarly apply to neurite extension. This insight may prove to be of therapeutic value for stimulating neuroregenerative processes.

Neurite extension occurs in parallel with growth cone guidance toward target cells. We presented evidence that SRF-directed gene expression is important for mossy fiber guidance (**Fig. 1**). In *Srf* mutants, mossy fibers aberrantly grew preferentially within the stratum pyramidale, rather than in a branched manner in the stratum lucidum (**Figs. 1** and **2**). This suggests a dominant repulsive guidance force in the wild-type hippocampus, which ensures mossy fiber navigation outside the stratum pyramidale, over an attractive force. After *Srf* deletion, the repulsive guidance mechanism seems to be selectively eliminated and a postulated—previously masked—attractive force now comes into effect. At present, the mechanisms leading to bifurcation and the subsequent guidance of mossy fibers outside the CA3 band are unknown. It is likely that the ingrowth of mossy fibers is prevented by both contact-mediated and chemorepulsive or attractive interactions of guidance receptors on mossy fibers with ligands localized to the stratum pyramidale (**Fig. 2**). SRF clearly is a key regulator in mossy fiber guidance, raising the question of which guidance cues at the axonal surface modulate SRF activity. So far, an *in vivo* function of axon guidance molecules in mossy fiber pathfinding has been indicated only for semaphorins, which are involved in the pruning of the infrapyramidal tract[27,34–36]. In agreement, our *in vitro* data (see below) suggest that SRF is crucial for the axonal repulsion induced by ephrin-As and semaphorins.

Mossy fiber terminals specifically target apical CA3 dendrites—localized in the stratum lucidum—to form excitatory glutamatergic synapses. We found that SRF-deficient mossy fiber terminals that had accumulated between CA3 cell bodies aberrantly synapsed onto CA3 somata and somatic spines, a location normally limited to inhibitory synapses (**Fig. 2**). These axosomatic (versus axodendritic) synapses may be more efficient—because of their proximity to the axon hillock—in driving neuronal discharge. Hippocampal long-term potentiation and activity-dependent gene induction are severely impaired in *Srf* mutants[16]. Hence it will be interesting to see the influence of SRF on learning and memory. Previous studies[37,38] have shown an inverse correlation between avoidance learning and infrapyramidal mossy fiber extension, which we found to be completely disturbed in *Srf* mutants (**Fig. 1**).

In this report, we described the formation of new ring-like structures consisting of both F-actin and microtubules in response to growth cone–collapsing stimuli was induced in *Srf* mutant neurons; these structures have not been described before (**Fig. 6**). In contrast to wild-type growth cones, SRF-deficient growth cones retained a polymerized F-actin status, indicative of impaired mechanisms of dynamic depolymerization. Not only the actin cytoskeleton, known to have a pivotal role in growth cone collapse, but also microtubule dynamics seemed to be affected in *Srf* mutants. Potential points of convergence mediating F-actin–microtubule cross-talk could be bispecific molecules such as the RhoA effector mDia or the Rho–guanine nucleotide exchange factor (GEF) GEF-H1, both of which influence SRF-mediated transcription[39].

The observed F-actin–microtubule rings may explain the insensitivity of SRF-deficient hippocampal growth cones to repulsive activities *in vitro* (**Fig. 5**) and may contribute toward the misrouting of mossy fibers *in vivo* (**Fig. 1**). Additional insensitivity of SRF-deficient neurons may be caused by the reduced expression of *Epha4*, *Epha7* and *Sema3c* (**Fig. 8**). The fact that F-actin–microtubule rings were retained after stimulation by both ephrins and semaphorins (**Fig. 6**) argues for shared signaling steps downstream of their cognate receptors (EphAs and neuropilin/plexin complexes). What cytoskeletal constituents might contribute to deregulated growth cone dynamics in SRF-deficient neurons? In a previous study[17], we demonstrated increased inhibitory phosphorylation of the F-actin depolymerizing/severing factor cofilin[26] in SRF-deficient brain cells. Decreased actin-severing activity of coffilin might contribute to the persistance of F-actin rings in growth cones after the induction of collapse. The mechanism leading to enhanced cofilin phosphorylation is unknown. Decreased phosphatase (slingshots, chronophin[40,41]) or enhanced LIM kinase, the latter resulting from elevated RhoA and ROCK activity, could account for cofilin phosphorylation. Notably, we found altered expression of Rho-GTPase signaling intermediates in SRF-deficient neurons like Rho-GEF5, a member of the ephexin subfamily of Rho-GEFs, which specifically interact with EphA receptors[42].

Besides the cytoskeletal impairments intrinsic to the SRF-deficient growth cone, guidance cues could trigger SRF-dependent gene expression, which would be disturbed in *Srf* mutants. Indeed, in wild-type neurons, stimulation by ephrin-A (data not shown) or ephrin-B (in combination with activation of glutamate receptors; ref. 43) resulted in the expression of selected SRF target genes.

Finally, here we identified the SRF cofactor MAL as a new mediator of neurite outgrowth and guidance. MAL can be viewed as an actin-binding sensor whose activity is intimately linked to the G- to F-actin ratio in cells. Thus, the functions of MAL in neurons might not be confined to the regulation of gene expression but could also be instrumental in the regulation of actin dynamics at the distally localized growth cone.

Our data and those of others[16,44–46] point toward a considerable contribution of gene expression to neurite outgrowth, axon guidance and synaptic targeting. It will be interesting to investigate how transcriptional regulation in the nuclear compartment is orchestrated in tune with the navigation of the growth cone.

METHODS

Mice. Mice carrying at least one functional *Srf* allele ($Srf^{f/f}$ or $Srf^{f/+;\,CamKII\alpha Cre}$) are referred to as control or wild-type mice. *Srf* mutants are abbreviated as $Srf^{f/f;\,CamKII\alpha Cre}$ (refs. 17, 19 and 20). Animal experiments and housing were in accordance with the guidelines of the Federation of European Laboratory Animal Science Associations and were approved by the local ethics committee (Tübingen University).

Materials. SRF plasmids were described in ref. 8. The constructs for Rho-GTPases were a gift from A. Püschel (University of Münster, Münster, Germany), for MAL from R. Treisman (Cancer Research UK, London), for β-actin from G. Posern (Max-Planck-Institut, Munich), and for semaphorin 3A and 4D from S. Offermanns (University of Heidelberg, Heidelberg, Germany) and L. Tamagnone (Torino, Italy). Antibodies and dilutions: mouse antibody to NFAP (1:50, Developmental Studies Hybridoma Bank), mouse antibody to calbindin (1:10,000, Swant), rabbit antibody to Tau (1:200, Chemicon), mouse antibody to Map2 (1:500, Chemicon), mouse antibody to β-tubulin (1:500, Sigma), rabbit antibody to Prox1 (1:500, Chemicon) and rabbit antibody to

synaptoporin (1:250, Synaptic Systems). Texas red–phalloidin (Molecular Probes) was used at 1:100 dilution.

Histology and EM. Protocols for histology and EM, and also for Timm staining and synaptoporin immo-EM, will be provided on request. Map2 and Tau staining was performed according to ref. 30.

Neuronal cell cultures. P1–P3 hippocampi or cerebellar cultures were prepared as described in ref. 47. Amaxa mouse neuron nucleofector solution was used as recommended by the manufacturer (Amaxa). A total of 3 μg DNA (2.25 μg construct + 0.75 μg green fluorescent protein (eGFP) vector) was used to electroporate cultures. Cultures were incubated 2 days *in vitro* (d.i.v.) (neurite outgrowth and guidance assays) or 8 d (neuronal polarization).

Neurite outgrowth assay. Acid-treated coverslips (diameter 13 mm) were coated with 100 μg ml^{-1} poly-L-lysin (Sigma) in borate buffer for 1 h at 37 °C, and were then washed and incubated with 20 μg ml^{-1} mouse laminin (Gibco), 20 μg ml^{-1} fibronectin (Becton Dickinson) or 50 μg ml^{-1} collagen (Becton Dickinson) in Hanks' balanced salt solution (HBSS) for 3–4 h at 37 °C. Neurons were plated at a density of 5×10^3–2×10^4 cells per coverslip.

Axon guidance assays. We performed stripe assays using recombinant ephrin-A5–Fc (R&D systems) and the Fc part of the human IgG alone (Calbiochem), as previously reported[48].

For growth cone collapse assays, cultures were incubated for 30 min at 37 °C with 1 μg ml^{-1} preclustered ephrin-A5–Fc (10 μg ml^{-1} anti-human IgG, Fc-specific for 30 min; Sigma) or Fc alone. Supernatants of semaphorin 3A– or semaphorin 4D–transfected HEK293 cells (or vector-transfected cells as control) were harvested 2 d after lipofectamine (Invitrogen) transfection and applied for 1 h (undiluted).

Real-time PCR analysis. Hippocampal cultures from P2–P3 mice were left for 2–3 d *in vitro*, followed by real-time PCR analysis as previously described[8]. Primer sequences are available on request.

Quantification and statistical analysis. Neurite length was determined using LSM image browserV3.2 (Zeiss) and ImageProPlus4.5 software (Media Cybernetics). The line profiles drawn spanned the maximal neurite length of a given neuron. Synapse quantification was performed as previously described[49,50]. In stripe assays, neurites that entered the ephrin-A5–containing stripe at any point were scored as not repelled. To quantify pixels using ImagePro software, we evaluated four random pictures of each mouse tested. To quantify growth cone collapse, only fully collapsed growth cones were scored. Growth cones bearing F-actin–microtubule rings, as seen for *Srf* mutants upon ephrin-A5 stimulation, were scored as not collapsed. In electroporation experiments, we quantified only GFP-positive neurons, nearly 100% of which also expressed the second electroporated construct in control experiments (data not shown). For any given result, at least three independent experiments were performed. For every mouse we analyzed 50–100 neurons for neurite outgrowth, 50–100 for the stripe assay, >20 for the growth cone collapse assay and 10–15 for neuronal polarization. For statistical analysis, P values were obtained with the two-tailed t-test. All bars represent mean values ± s.d. Asterisks indicate statistical significance with $^*P \leq 0.05$, $^{**}P \leq 0.01$ and $^{***}P \leq 0.001$.

Note: Supplementary information is available on the Nature Neuroscience website.

ACKNOWLEDGMENTS

We thank B. Habermehl, M. Koch, B. Joch and D. Steuerwald for experimental help and T. Skutella for discussions. We received financial aid from the Deutsche Forschungsgemeinschaft (120/12-1, SFB 446 and SFB 505) and the Fonds der Chemischen Industrie.

AUTHOR CONTRIBUTIONS

B.K. designed and performed all experiments, analyzed the data and wrote the manuscript. O.K. designed and performed the experiment shown in **Figure 2** and **Supplementary Figure 2**. C.F. contributed to the experiments shown in **Figure 8**. S.A. was involved in breeding *Srf* mutants. G.S. provided the CamKIIα-Cre mice. M.F. provided technical and intellectual expertise. A.N. provided technical and intellectual expertise and wrote the manuscript.

COMPETING INTERESTS STATEMENT

The authors declare that they have no competing financial interests.

Published online at http://www.nature.com/natureneuroscience/
Reprints and permissions information is available online at http://npg.nature.com/reprintsandpermissions/

1. Nicoll, R.A. & Malenka, R.C. Contrasting properties of two forms of long-term potentiation in the hippocampus. *Nature* **377**, 115–118 (1995).
2. Morimoto, K., Fahnestock, M. & Racine, R.J. Kindling and status epilepticus models of epilepsy: rewiring the brain. *Prog. Neurobiol.* **73**, 1–60 (2004).
3. Blackstad, T.W. & Kjaerheim, A. Special axo-dendritic synapses in the hippocampal cortex: electron and light microscopic studies on the layer of mossy fibers. *J. Comp. Neurol.* **117**, 133–159 (1961).
4. Norman, C., Runswick, M., Pollock, R. & Treisman, R. Isolation and properties of cDNA clones encoding SRF, a transcription factor that binds to the c-fos serum response element. *Cell* **55**, 989–1003 (1988).
5. Wang, D.Z. & Olson, E.N. Control of smooth muscle development by the myocardin family of transcriptional coactivators. *Curr. Opin. Genet. Dev.* **14**, 558–566 (2004).
6. Cen, B., Selvaraj, A. & Prywes, R. Myocardin/MKL family of SRF coactivators: key regulators of immediate early and muscle specific gene expression. *J. Cell. Biochem.* **93**, 74–82 (2004).
7. Buchwalter, G., Gross, C. & Wasylyk, B. Ets ternary complex transcription factors. *Gene* **324**, 1–14 (2004).
8. Schratt, G. *et al.* Serum response factor is crucial for actin cytoskeletal organization and focal adhesion assembly in embryonic stem cells. *J. Cell Biol.* **156**, 737–750 (2002).
9. Somogyi, K. & Rorth, P. Evidence for tension-based regulation of *Drosophila* MAL and SRF during invasive cell migration. *Dev. Cell* **7**, 85–93 (2004).
10. Sotiropoulos, A., Gineitis, D., Copeland, J. & Treisman, R. Signal-regulated activation of serum response factor is mediated by changes in actin dynamics. *Cell* **98**, 159–169 (1999).
11. Hill, C.S., Wynne, J. & Treisman, R. The Rho family GTPases RhoA, Rac1, and CDC42Hs regulate transcriptional activation by SRF. *Cell* **81**, 1159–1170 (1995).
12. Etienne-Manneville, S. & Hall, A. Rho GTPases in cell biology. *Nature* **420**, 629–635 (2002).
13. Miralles, F., Posern, G., Zaromytidou, A.I. & Treisman, R. Actin dynamics control SRF activity by regulation of its coactivator MAL. *Cell* **113**, 329–342 (2003).
14. Philippar, U. *et al.* The SRF target gene Fhl2 antagonizes RhoA/MAL-dependent activation of SRF. *Mol. Cell* **16**, 867–880 (2004).
15. Xia, Z., Dudek, H., Miranti, C.K. & Greenberg, M.E. Calcium influx via the NMDA receptor induces immediate early gene transcription by a MAP kinase/ERK-dependent mechanism. *J. Neurosci.* **16**, 5425–5436 (1996).
16. Ramanan, N. *et al.* SRF mediates activity-induced gene expression and synaptic plasticity but not neuronal viability. *Nat. Neurosci.* **8**, 759–767 (2005).
17. Alberti, S. *et al.* Neuronal migration in the murine rostral migratory stream requires serum response factor. *Proc. Natl. Acad. Sci. USA* **102**, 6148–6153 (2005).
18. Arsenian, S., Weinhold, B., Oelgeschlager, M., Ruther, U. & Nordheim, A. Serum response factor is essential for mesoderm formation during mouse embryogenesis. *EMBO J.* **17**, 6289–6299 (1998).
19. Wiebel, F.F., Rennekampff, V., Vintersten, K. & Nordheim, A. Generation of mice carrying conditional knockout alleles for the transcription factor SRF. *Genesis* **32**, 124–126 (2002).
20. Casanova, E. *et al.* A CamKIIalpha iCre BAC allows brain-specific gene inactivation. *Genesis* **31**, 37–42 (2001).
21. Singec, I. *et al.* Synaptic vesicle protein synaptoporin is differently expressed by subpopulations of mouse hippocampal neurons. *J. Comp. Neurol.* **452**, 139–153 (2002).
22. Pasquale, E.B. Eph receptor signalling casts a wide net on cell behaviour. *Nat. Rev. Mol. Cell Biol.* **6**, 462–475 (2005).
23. Brownlee, H. *et al.* Multiple ephrins regulate hippocampal neurite outgrowth. *J. Comp. Neurol.* **425**, 315–322 (2000).
24. Murai, K.K., Nguyen, L.N., Irie, F., Yamaguchi, Y. & Pasquale, E.B. Control of hippocampal dendritic spine morphology through ephrin-A3/EphA4 signaling. *Nat. Neurosci.* **6**, 153–160 (2003).
25. Hansen, M.J., Dallal, G.E. & Flanagan, J.G. Retinal axon response to ephrin-as shows a graded, concentration-dependent transition from growth promotion to inhibition. *Neuron* **42**, 717–730 (2004).
26. Dent, E.W. & Gertler, F.B. Cytoskeletal dynamics and transport in growth cone motility and axon guidance. *Neuron* **40**, 209–227 (2003).
27. Chedotal, A. *et al.* Semaphorins III and IV repel hippocampal axons via two distinct receptors. *Development* **125**, 4313–4323 (1998).
28. Swiercz, J.M., Kuner, R., Behrens, J. & Offermanns, S. Plexin-B1 directly interacts with PDZ-RhoGEF/LARG to regulate RhoA and growth cone morphology. *Neuron* **35**, 51–63 (2002).
29. Govek, E.E., Newey, S.E. & Van Aelst, L. The role of the Rho GTPases in neuronal development. *Genes Dev.* **19**, 1–49 (2005).
30. Schwamborn, J.C. & Puschel, A.W. The sequential activity of the GTPases Rap1B and Cdc42 determines neuronal polarity. *Nat. Neurosci.* **7**, 923–929 (2004).
31. Da Silva, J.S. *et al.* RhoA/ROCK regulation of neuritogenesis via profilin IIa-mediated control of actin stability. *J. Cell Biol.* **162**, 1267–1279 (2003).
32. Tabuchi, A. *et al.* Nuclear translocation of the SRF co-activator MAL in cortical neurons: role of RhoA signalling. *J. Neurochem.* **94**, 169–180 (2005).

33. Yue, Y. *et al.* Mistargeting hippocampal axons by expression of a truncated Eph receptor. *Proc. Natl. Acad. Sci. USA* **99**, 10777–10782 (2002).
34. Bagri, A., Cheng, H.J., Yaron, A., Pleasure, S.J. & Tessier-Lavigne, M. Stereotyped pruning of long hippocampal axon branches triggered by retraction inducers of the semaphorin family. *Cell* **113**, 285–299 (2003).
35. Chen, H. *et al.* Neuropilin-2 regulates the development of selective cranial and sensory nerves and hippocampal mossy fiber projections. *Neuron* **25**, 43–56 (2000).
36. Cheng, H.J. *et al.* Plexin-A3 mediates semaphorin signaling and regulates the development of hippocampal axonal projections. *Neuron* **32**, 249–263 (2001).
37. Lipp, H.P., Schwegler, H., Heimrich, B. & Driscoll, P. Infrapyramidal mossy fibers and two-way avoidance learning: developmental modification of hippocampal circuitry and adult behavior of rats and mice. *J. Neurosci.* **8**, 1905–1921 (1988).
38. Lipp, H.P. *et al.* Using genetically-defined rodent strains for the identification of hippocampal traits relevant for two-way avoidance behavior: a non-invasive approach. *Experientia* **45**, 845–859 (1989).
39. Krendel, M., Zenke, F.T. & Bokoch, G.M. Nucleotide exchange factor GEF-H1 mediates cross-talk between microtubules and the actin cytoskeleton. *Nat. Cell Biol.* **4**, 294–301 (2002).
40. Niwa, R., Nagata-Ohashi, K., Takeichi, M., Mizuno, K. & Uemura, T. Control of actin reorganization by Slingshot, a family of phosphatases that dephosphorylate ADF/cofilin. *Cell* **108**, 233–246 (2002).
41. Gohla, A., Birkenfeld, J. & Bokoch, G.M. Chronophin, a novel HAD-type serine protein phosphatase, regulates cofilin-dependent actin dynamics. *Nat. Cell Biol.* **7**, 21–29 (2005).
42. Shamah, S.M. *et al.* EphA receptors regulate growth cone dynamics through the novel guanine nucleotide exchange factor ephexin. *Cell* **105**, 233–244 (2001).
43. Takasu, M.A., Dalva, M.B., Zigmond, R.E. & Greenberg, M.E. Modulation of NMDA receptor-dependent calcium influx and gene expression through EphB receptors. *Science* **295**, 491–495 (2002).
44. Graef, I.A. *et al.* Neurotrophins and netrins require calcineurin/NFAT signaling to stimulate outgrowth of embryonic axons. *Cell* **113**, 657–670 (2003).
45. Lonze, B.E., Riccio, A., Cohen, S. & Ginty, D.D. Apoptosis, axonal growth defects, and degeneration of peripheral neurons in mice lacking CREB. *Neuron* **34**, 371–385 (2002).
46. Rudolph, D. *et al.* Impaired fetal T cell development and perinatal lethality in mice lacking the cAMP response element binding protein. *Proc. Natl. Acad. Sci. USA* **95**, 4481–4486 (1998).
47. Goetze, B., Grunewald, B., Baldassa, S. & Kiebler, M. Chemically controlled formation of a DNA/calcium phosphate coprecipitate: application for transfection of mature hippocampal neurons. *J. Neurobiol.* **60**, 517–525 (2004).
48. Rashid, T. *et al.* Opposing gradients of ephrin-As and EphA7 in the superior colliculus are essential for topographic mapping in the mammalian visual system. *Neuron* **47**, 57–69 (2005).
49. Sterio, D.C. The unbiased estimation of number and sizes of arbitrary particles using the disector. *J. Microsc.* **134**, 127–136 (1984).
50. Braendgaard, H. & Gundersen, H.J. The impact of recent stereological advances on quantitative studies of the nervous system. *J. Neurosci. Methods* **18**, 39–78 (1986).